Amino Acids (2015) 47:1567–1577
DOI 10.1007/s00726-015-1998-x

ORIGINAL ARTICLE

The N-terminal cytoplasmic domain of neuregulin 1 type III is intrinsically disordered

Maryna Chukhlieb[1] · Arne Raasakka[1,2] · Salla Ruskamo[1] · Petri Kursula[1,2]

Received: 1 April 2015 / Accepted: 21 April 2015 / Published online: 6 May 2015

Abstract Axonally expressed neuregulin 1 (NRG1) type III is a transmembrane protein involved in various neurodevelopmental processes, including myelination and Schwann cell migration. NRG1 type III has one transmembrane domain and a C-terminal extracellular segment, which contains an epidermal growth factor homology domain. Little is known, however, about the intracellular N terminus of NRG1 type III, and the structure–function relationships of this cytoplasmic domain have remained uncharacterized. In the current study, we carried out the first structural and functional studies on the NRG1 type III cytoplasmic domain. Based on sequence analyses, the domain is predicted to be largely disordered, while a strictly conserved region close to the transmembrane segment may contain helical structure and bind metal ions. As shown by synchrotron radiation circular dichroism spectroscopy, the recombinant NRG1 type III cytoplasmic domain was disordered in solution, but it was able to fold partially into a helical structure, especially when both metals and membrane-mimicking compounds were present. NRG1 cytoplasmic tail binding to metals was further confirmed by calorimetry. These results suggest that the juxtamembrane segment of the NRG1 type III cytoplasmic domain may fold onto the membrane surface upon metal binding. Using synchrotron small-angle X-ray scattering, we further proved that the NRG1 cytoplasmic domain is intrinsically disordered, highly elongated, and behaves like a random polymer. Our work provides the first biochemical and biophysical data on the previously unexplored cytoplasmic domain of NRG1 type III, which will help elucidate the detailed structure–function relationships of this domain.

Keywords Myelin · Neuregulin · Intrinsically disordered proteins · Metal binding · Membrane · Protein structure

Introduction

Myelin is a protective proteolipid multilayer wrapped around axons, which speeds up nerve impulse conduction. Myelination is important for the normal functioning of the nervous system, and the loss of myelin may cause neurodegenerative disease. There are two types of myelin-forming cells: oligodendrocytes in the central nervous system and Schwann cells in the peripheral nervous system. Myelination by these glial cells is under tight control, and axonal signals play a key role during different phases of myelin formation. On the other hand, signals produced by Schwann cells are responsible for the maintenance of neurons (Garratt et al. 2000).

Neuregulin (NRG) is a neuronal protein, which regulates various developmental processes, mainly through its extracellular epidermal growth factor (EGF) homology domain that binds to tyrosine kinase receptors on the myelinating Schwann cell (Falls 2003a). There are at least 15 different isoforms of neuregulin 1 (NRG1) (Falls 2003b). Axonally derived NRG1 type III is required for the survival and growth of Schwann cells in peripheral nerves and plays a key role in their development, all the way from neural crest cells through Schwann cell precursors to myelinating or non-myelinating Schwann cells. The importance of the NRG1 type III signalling system in Schwann cell

✉ Petri Kursula
petri.kursula@biomed.uib.no

[1] Faculty of Biochemistry and Molecular Medicine, Biocenter Oulu, University of Oulu, Oulu, Finland

[2] Department of Biomedicine, University of Bergen, Bergen, Norway

development was confirmed in studies on mice lacking ErbB3 receptors (Erickson et al. 1997). Axonally derived NRG1 type III is also important for the regulation of myelin thickness (Michailov et al. 2004). Knockout studies on mice implicate an important role for the NRG1 signalling system in the development of glia in the central nervous system, and the lack of NRG1 causes abnormal myelin thickness and may be related to different neurological diseases, such as schizophrenia (Karl 2013; Mei and Xiong 2008). It has also been suggested that abnormal expression of NRG1 type III may be linked to schizophrenia (Weickert et al. 2012).

Seminal studies on NRG1 type III have also been conducted using zebrafish models, which allow to follow Schwann cell migration and peripheral nerve myelination in great detail. A point mutation has also been characterized, affecting the transmembrane domain, which leads to myelination defects in zebrafish (Perlin et al. 2011). The mechanism for these defects relates to Schwann cell migration, and also axonal recognition may have played a role. In a mammalian cell culture model, the results pointed towards an effect of NRG1 type III on Schwann cell survival rather than on migration (Heermann and Schwab 2013). A model involving gradients in NRG1 type III concentration on the axonal plasma membrane during Schwann cell migration, axonal recognition, and myelination has been proposed (Nave and Salzer 2006; Perlin et al. 2011).

The N-terminal region of NRG1 type III was originally thought to represent an extracellular domain; however, it is clear now that this domain has a transmembrane segment, and the most N-terminal region is cytoplasmic (Wang et al. 2001). While research has been carried out on the C-terminal cytoplasmic domain of NRG1, which is cleaved off during NRG1 type III maturation (Fleck et al. 2013), no biochemical, biophysical, functional, or structural studies exist to our knowledge on the N-terminal cytoplasmic domain, which remains an integral part of the transmembrane protein on the neuronal surface. The extracellular domain can also further be released by proteolytic cleavage to produce a paracrine signal (Fleck et al. 2013). The N-terminal cytoplasmic domain harbours a cysteine-rich domain (CRD), which consists of conserved cysteine residues in the transmembrane helix and in the C-terminal end of the cytoplasmic domain, close to the membrane. NRG1 type III is the only neuregulin isoform having a CRD.

In this study, we carried out structural characterization of recombinantly produced NRG1 type III N-terminal cytoplasmic domain (NRG1-III-Nct). The results strongly suggest an intrinsically disordered structure for NRG1-III-Nct. Metal binding by the cytoplasmic domain was verified by different techniques, and it is likely that metal and membrane binding are connected to partial folding of this domain.

Experimental methods

Protein sequence analysis

Various methods were used to predict the structural properties of NRG1-III-Nct. Secondary structure predictions were carried out with PSIPRED (Buchan et al. 2013) and structural disorder was analysed using GlobPlot (Linding et al. 2003), DISOPRED (Jones and Cozzetto 2015), and PONDR (Romero et al. 2004). Molecular modelling was carried out using Phyre2 (Bennett-Lovsey et al. 2008).

Expression vector preparation

Full-length human NRG1 type III cDNA (amino acids 1–285), optimized for *E. coli* expression, was purchased from Eurofins MWG Operon (Ebersberg, Germany) and used for subcloning the N-terminal cytoplasmic domain cDNA (amino acids 1–75) of NRG1 type III into the pTH27 expression vector (Hammarström et al. 2006) with a Tobacco Etch Virus (TEV) protease cleavage site. The expression construct was verified by DNA sequencing.

Protein expression and purification

The hexahistidine-tagged NRG1-III-Nct fusion protein was expressed in *E. coli* BL21(DE3) cells, grown in Terrific Broth (TB) medium with 100 µg/ml ampicillin. The cells were incubated at +37 °C until the OD_{600} was 0.6–0.8, and protein expression was started by adding 0.4 mM isopropyl β-D-1-thiogalactopyranoside (IPTG). Induction was carried out for 4 h at +37 °C. The cells were harvested by centrifugation, resuspended in cold lysis buffer (50 mM Tris–HCl pH 7.5, 150 mM NaCl, 1 mM dithiothreitol (DTT)), and stored at −70 °C.

Cells lysis was performed by sonication, and debris was removed by centrifugation at 20,000 g for 30 min. The supernatant was applied onto a 1-ml Ni-NTA column, pre-equilibrated with cold washing buffer (50 mM Tris–HCl pH 7.5, 150 mM NaCl, 30 mM imidazole). The protein was eluted with elution buffer (50 mM Tris–HCl pH 7.5, 150 mM NaCl, 250 mM imidazole), and TEV protease (van den Berg et al. 2006) cleavage was performed overnight at +4 °C with constant mixing. The cleavage reaction was simultaneously dialysed against 20 mM Tris–HCl pH 7.5, 150 mM NaCl, 1 mM DTT. To remove excess TEV protease and the tag, the cleaved protein was again applied onto a Ni-NTA column, and the flow-through was collected. The protein was concentrated and further purified by size exclusion chromatography (SEC) using a HiLoad 16/60 Superdex 75 pg column (GE Healthcare) equilibrated with running buffer (20 mM Tris–HCl pH 7.5, 150 mM NaCl, 1 mM DTT). The fractions containing

NRG1-III-Nct, as confirmed by SDS-PAGE, were pooled, concentrated, flash frozen in liquid nitrogen, and stored at −70 °C until further use.

Mass spectrometry

Correct identity of the purified recombinant protein was verified by tryptic peptide mapping and MALDI-TOF mass spectrometry using an Ultra fleXtreme mass spectrometer (Bruker). Accurate molecular weight determination and disulphide bond analysis of NRG1-III-Nct were performed by liquid reverse-phase chromatography coupled electrospray ionization time-of-flight mass spectrometry (ESI-TOF MS), using an Acquity UPLC coupled Synapt G2 mass spectrometer (Waters).

Static light scattering

Molecular weight of NRG1-III-Nct was determined by analytical SEC using a Superdex 75 pg 10/300 GL column (GE Healthcare) coupled to a Shimadzu liquid chromatography system. A mini-DAWN TREOS multi-angle static light scattering (SLS) detector (Wyatt) and a Shimadzu refractive index detector for absolute molecular weight determination were used. Data were analysed using the ASTRA software (Wyatt). The running buffer was 20 mM Tris–HCl (pH 7.5), 150 mM NaCl.

Circular dichroism spectroscopy

Synchrotron radiation circular dichroism (SRCD) data were collected on synchrotron radiation beamlines UV-CD12 at ANKA (Karlsruhe, Germany) and DISCO (Refregiers et al. 2012) at SOLEIL (Paris, France). The monomeric protein sample was dialysed in advance into water containing 0.5 mM of the reducing agent tris(2-carboxyethyl)phosphine (TCEP). SRCD spectra were collected in the wavelength range of 170–280 nm using 10-to-100-µm pathlength quartz cuvettes. The protein was studied in the presence of 10–50 % (v/v) trifluoroethanol (TFE), 5 mM $ZnCl_2$, 5 mM $NiCl_2$, 5 mM $CuCl_2$, 0.1 % dodecyl phosphocholine (DPC), 0.5 % sodium dodecyl sulphate (SDS), a 1:1 mixture of 3 mM dioleoyl phosphatidylcholine (DOPC) and dioleoyl phosphatidylserine (DOPS), and a 1:1 mixture of 3 mM dimyristoyl phosphatidylcholine (DMPC) and dimyristoyl phosphatidylglycerol (DMPG).

Additional in-house CD measurements were carried out using a Chirascan Plus CD spectropolarimeter (Applied Photophysics). The protein was studied in the presence of 0.1 % DPC, 0.5 % SDS, 5 mM $NiCl_2$, 5 mM $MgSO_4$, 5 mM Na_2SO_4, 5 mM $CaCl_2$, 5 mM $CoCl_2$, 5 mM $CuCl_2$, and a 1:1 mixture of 3 mM DMPC and DMPG.

Isothermal titration calorimetry

Isothermal titration calorimetry (ITC) was performed using the ITC200 instrument (GE Healthcare) at +25 °C. The protein was dialysed into the assay buffer (20 mM Tris–HCl pH 7.5, 150 mM NaCl, 0.5 mM TCEP). The titration was done by injecting 2.5-µL aliquots of the metal ($ZnCl_2$, $NiSO_4$, $MgCl_2$, $Fe_2(SO_4)_3$) from the syringe (concentration 300 µM) into the protein sample in the measurement cell (concentration 30 µM) 16 times, at time intervals of 120 s. The data were analysed using Origin 7.0 and fitted by the one-site binding model.

Small-angle X-ray scattering

Small-angle X-ray scattering (SAXS) data were collected on the SWING small-angle X-ray scattering beamline (David and Pérez 2009) at SOLEIL (Paris, France) synchrotron, in 20 mM Tris–HCl pH 7.5, 150 mM NaCl. The protein samples used for the online SEC-SAXS measurements were symmetric peaks on SEC, corresponding to monomeric and dimeric protein forms. For the batch measurements, the protein concentration ranged between 3 and 12 mg/ml. Initial data processing was carried out with the program Foxtrot. The data were further processed and analysed with the ATSAS suite (Petoukhov et al. 2012). GNOM was used for calculating the distance distribution function (Svergun 1992). Protocols based on Debye formalism, better suited for intrinsically disordered molecules, were also employed in estimating R_g (Calmettes et al. 1994). Ab initio chain-like models were built using GASBOR (Svergun et al. 2001). Ab initio modelling was also done using the program Denfert (Koutsioubas and Pérez 2013), which additionally models a hydration layer around the protein. The protein is represented in this case by dummy atoms. Conformational ensembles were fitted using EOM (Bernado et al. 2007). The molecular weight of the protein was estimated from the volume of the ab initio models, assuming a specific volume of 0.7425 $cm^3\ g^{-1}$ (Mylonas and Svergun 2007). As this value has been determined for globular proteins, it is likely to slightly overestimate molecular weights of disordered proteins.

Results and discussion

While some research has been carried out on the C-terminal cytoplasmic domain of NRG1 (Liu et al. 1998a, b; Velanac et al. 2012; Wang et al. 1998; Zhang et al. 2006), the N-terminal cytosolic segment of the transmembrane NRG1 type III, sitting on the neuronal plasma membrane (Fig. 1a), has received no attention. We produced the N-terminal cytoplasmic domain of NRG1 type III recombinantly

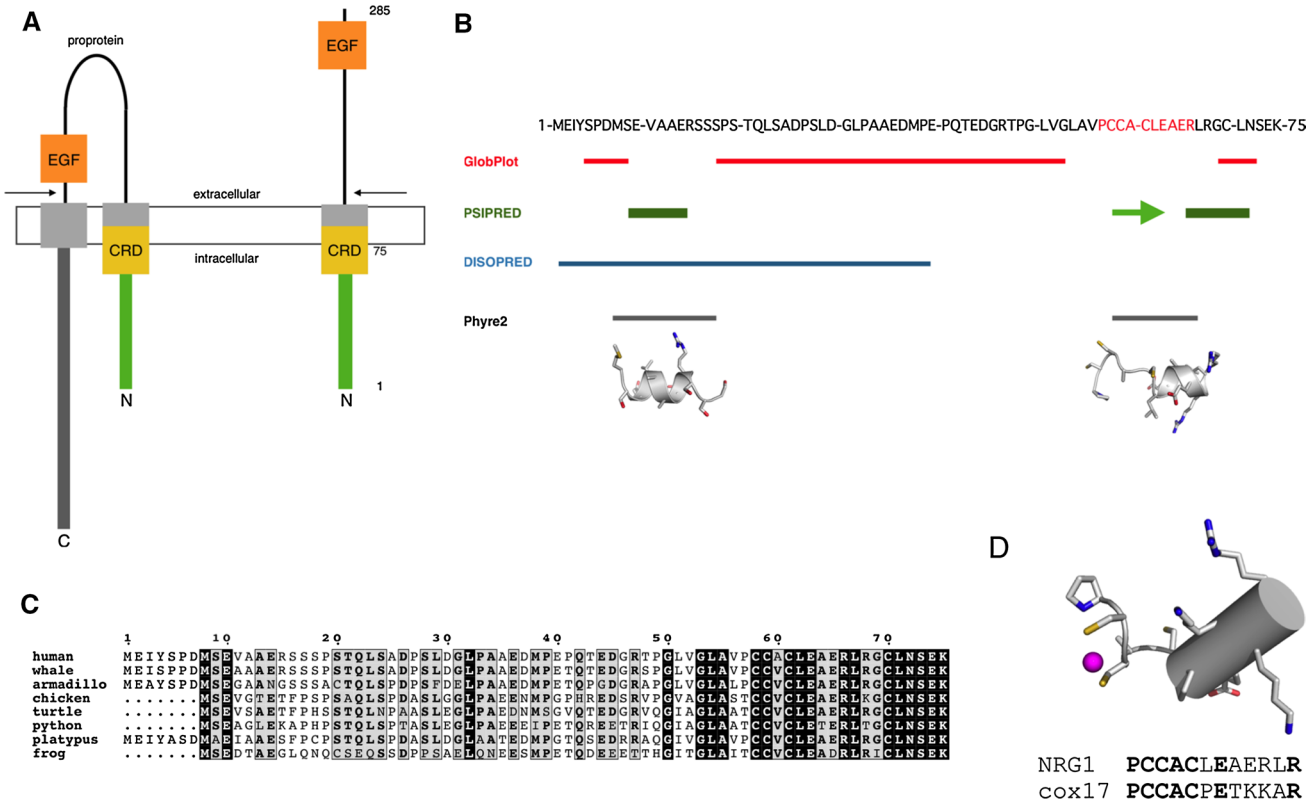

Fig. 1 The overall structure of NRG1 type III A. **a** Schematic view of the processing of NRG1 type III. The *arrows* indicate sites of proteolytic processing. The extracellular domain of NRG1 type III (*right*) can also be released by proteolysis, although the protein is mainly thought to be functional in its transmembrane form. **b** Sequence analysis of NRG1-III-Nct. Below the sequence, predicted disordered (GlobPlot/DISOPRED) and ordered (PSIPRED/Phyre2) regions are shown, together with Phyre2 models for the ordered segments. **c** Alignment of NRG1-III-Nct from different species shows strict conservation of the C-terminal CRD segment. **d** The structure of the copper-binding site in Cox17 (Banci et al. 2008), where the metal is coordinated by two vicinal Cys residues. The alignment between NRG1-III-Nct and Cox17 in the region shown in the figure is also given

and carried out a biochemical and biophysical characterization to show NRG1-III-Nct is an intrinsically disordered protein (IDP). The possible interactions of this domain with membranes were also examined, as was a predicted metal-binding site close to the membrane.

Sequence analysis and structural predictions suggest intrinsic disorder

As a first step in the structural analysis of the NRG1-III-Nct, we used various bioinformatics tools. As far as predicted secondary structure is concerned, one helical region is predicted close to the C terminus of the domain (near the transmembrane domain) (amino acids 58–69), and another one near the N terminus (amino acids 9–19) (Fig. 1b). Disorder prediction methods all agree that NRG1-III-Nct is mainly disordered, with some possibly ordered regions coinciding with those detected in secondary structure prediction (Fig. 1b). Comparing NRG1-III-Nct sequences from various animal species (Fig. 1c), it is evident that the C-terminal end of the cytoplasmic domain is nearly fully conserved, while there is more variation in the N-terminal half. This suggests that the C-terminal segment of NRG1-III-Nct is structurally or functionally important. Furthermore, homology modelling was attempted using Phyre2. Interestingly, close sequence motif matches to a metal-binding site from Cox17 (Banci et al. 2008) were detected in the CRD, which is predicted to be helical near the membrane (amino acids 58–69) (Fig. 1d).

Taking the results from sequence analysis together, NRG1-III-Nct is likely to be an IDP, which may have some propensity to fold. Folding could be affected by e.g. the presence of metals or a membrane surface. For more insight into the molecular properties of NRG1-III-Nct, we carried out structural characterization in vitro.

Production of recombinant NRG1 type III N-terminal cytoplasmic domain

To experimentally study the NRG1-III-Nct structure, it (amino acids 1–75) was expressed and purified

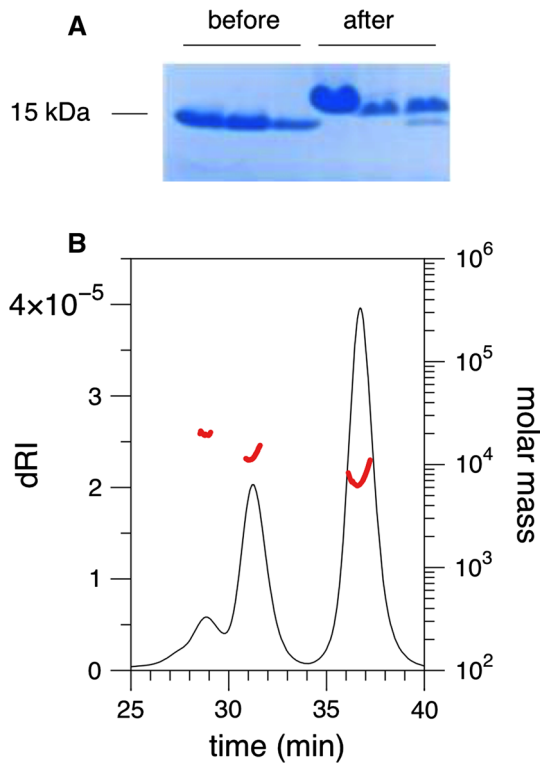

Fig. 2 Purification and oligomeric status of NRG1-III-Nct **a** SDS-PAGE analysis of purified NRG1-III-Nct with and without the His-tag. The mobility of the protein is decreased after tag cleavage. **b** SEC routinely separated monomeric and dimeric forms, and the protein is pure as judged by SDS-PAGE. Online SLS analysis was used to determine absolute molecular weights (*red*) for the SEC peaks (*left to right* trimer, dimer, monomer) (colour figure online)

recombinantly. The construct was designed to stop right before the transmembrane region (amino acids 76–100). Soluble NRG1-III-Nct was expressed in large amounts, and could be obtained in high purity (Fig. 2). The N-terminally hexahistidine-tagged fusion protein was initially purified by Ni-affinity chromatography followed by SEC. Atypical mobility of pure NRG1-III-Nct on SDS-PAGE was observed (Fig. 2a), which is an indication of a disordered nature of the protein. Also in our previous studies on another IDP, juxtanodin, lower mobility on SDS-PAGE than expected from molecular weight was observed (Ruskamo et al. 2012). The phenomenon is a general feature of IDPs, due to an overall lack of hydrophobic residues and the binding of less SDS than globular proteins. In addition, the recombinant protein moved even slower on SDS-PAGE after tag cleavage (Fig. 2a). As these samples were mainly monomers in SEC after cleavage (Fig. 2b), this behaviour reflects an additional increase in the abnormal mobility of NRG1-III-ct rather than dimerization. The identity of all protein bands was confirmed by mass spectrometric analysis of tryptic peptides (data not shown).

Static light scattering shows the presence of different oligomeric states

The oligomeric state of NRG1-III-Nct in solution was further investigated using SEC in combination with SLS (SEC–SLS). The protein eluted as three peaks (Fig. 2b). The molecular weight of each peak was determined, and they correspond to monomers (7.3 kDa), dimers (12.2 kDa), and trimers (19.8 kDa). The theoretical value, 7.9 kDa, for monomeric NRG1-III-Nct corresponds well to these experimental values. The results indicate the presence of mainly monomer and dimer in solution. Based on peak height, most of the protein was monomeric, and there was very little trimer. These results suggest an equilibrium between monomer and dimer in preparations of NRG1-III-Nct. This equilibrium could be shifted in the direction of a monomeric species by including DTT in the buffer, while its absence resulted in the accumulation of a dimeric species in SEC (data not shown).

As sequence analysis suggested no coiled-coil regions (data not shown), dimerization by disulphide bond formation was analysed by determination of the absolute molecular weight of the protein in the presence and absence of the reducing agent DTT, using ESI-TOF MS. After treating the protein with DTT for 20 min at room temperature, the protein was present only as monomer (7937.1 Da); before treatment, a mixture of monomers and dimers was observed (7934.1 and 15,869.9 Da, respectively). As a conclusion, dimerization of recombinant NRG1-III-Nct happens due to the formation of intermolecular disulphide bonds. This is likely an artefact from prolonged storage of the concentrated recombinant protein with free, reactive Cys residues. In most further experiments, reducing agent was used in all buffers to avoid disulphide bond formation and, hence, dimerization.

CD spectroscopy indicates disorder and induced partial folding

The folding of NRG1-III-Nct was studied by SRCD spectroscopy. In aqueous solution, the protein showed a typical spectrum for disordered proteins, with a strong negative minimum at 200 nm (Fig. 3a). This result fits well to the sequence-based predictions of disorder (Fig. 1b).

Since NRG1-III-Nct is located close to the neuronal plasma membrane in vivo, we further studied its membrane interactions using CD spectroscopy in membrane-mimicking conditions, with the assumption that membrane binding should lead to detectable conformational changes. Such changes have been seen for various membrane-interacting IDPs (Lazarova et al. 2004; Muruganandam et al. 2013; Myllykoski et al. 2012; Piirainen et al. 2015; Popovic et al. 2007; Sigalov and Hendricks 2009; Vassall et al. 2015;

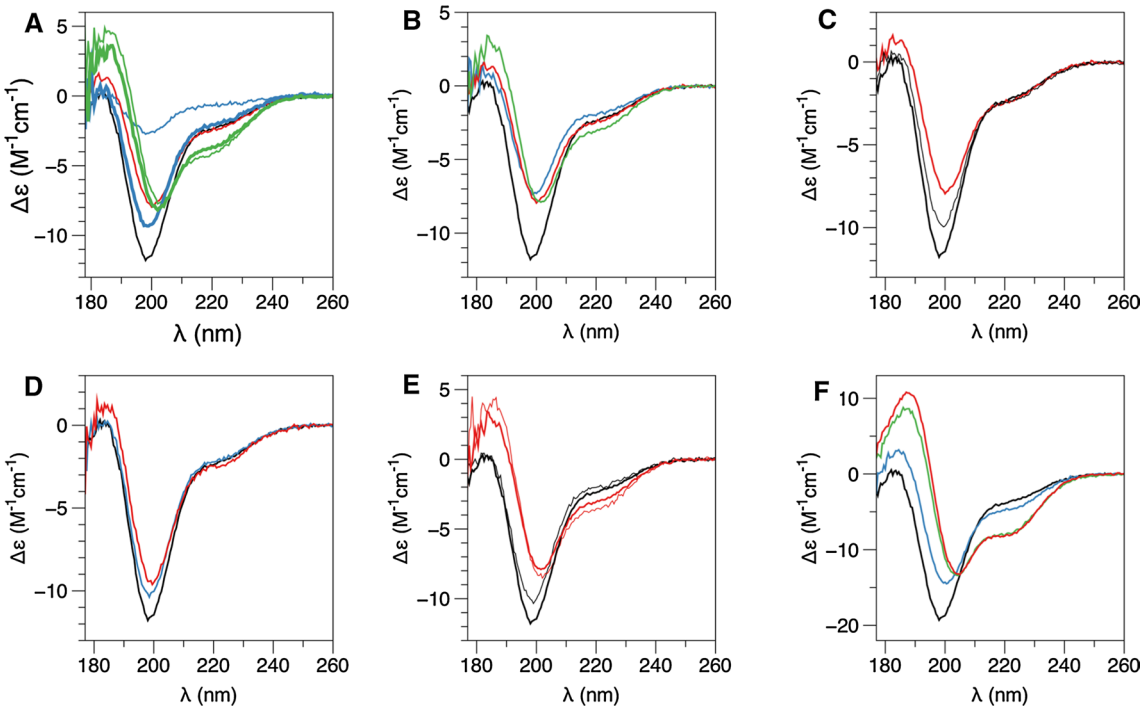

Fig. 3 Conformation of NRG1-III-Nct studied by SRCD spectroscopy **a** The combined effect of Ni^{2+} or Cu^{2+} and SDS on NRG1-III-Nct folding. *Black*, no additives; *red*, 0.5 % SDS; *thin blue*, 5 mM $CuCl_2$; *thin green*, $CuCl_2$ + SDS; *thick blue*, 5 mM $NiCl_2$; *thick green*, $NiCl_2$ + SDS. **b** The effect of Zn^{2+}. *Black*, no additives; *red*, 0.5 % SDS; *blue*, 5 mM $ZnCl_2$; *green*, $ZnCl_2$ + SDS. **c** The effect of 0.5 % SDS (*red*) and 0.1 % DPC (*thin black*) compared to protein in buffer (*thick black*). **d** NRG1-III-Nct alone (*black*), in 1:1 DMPC/DMPG (*blue*), and in 1:1 DMPC/DMPG with 5 mM $ZnCl_2$ (*red*). **e** SRCD spectra of NRG1-III-Nct with (*thick lines*) and without (*thin lines*) reducing agent. Samples in 0.5 % SDS, 5 mM $ZnCl_2$ are shown in *red*. **f** NRG1-III-Nct titrated with TFE. *Black*, *blue*, *green*, and *red* denote 0, 10, 30, and 50 % TFE, respectively (colour figure online)

Vasudevan et al. 2010; Wang et al. 2011). In the native NRG1 type III protein, the transmembrane domain will follow directly after the construct used here, so at least the C-terminal end of the NRG1-III-Nct will lie very close to the membrane surface in vivo.

As bioinformatics tools predicted a metal-binding site in the protein sequence (Fig. 1d), the influence of several metals, including zinc, nickel, sodium, copper, cobalt, magnesium and calcium on NRG1 folding was tested. NRG1-III-Nct turned out to be partially folded into α helices in the combined presence of 0.5 % SDS and either $ZnCl_2$, $NiCl_2$, or $CuCl_2$ at 5 mM (Fig. 3a, b). Metals or SDS alone caused less pronounced effects on the SRCD spectra. In the CD spectra, the negative minimum at 200 nm shifted towards a higher wavelength, and the negative minimum at 220 nm, presenting as a shoulder in mainly disordered samples, became more pronounced (Fig. 3a, b). These are hallmarks of an IDP gaining secondary structure, and have been detected for several IDPs, including juxtanodin (Ruskamo et al. 2012) and myelin basic protein (MBP) (Murugananadam et al. 2013). Furthermore, as a specific advantage of synchrotron CD, the very sensitive reaction of the CD peak around 185–190 nm towards even minor conformational changes could be observed in NRG1-III-Nct.

The above data indicated the possibility of NRG1 binding to metal ions. The protein with metals alone remained mainly unfolded, but the spectra changed in the combined presence of detergent (0.5 % SDS) and metals (Fig. 3a, b). SDS alone induced some folding (Fig. 3c), but no such effect was seen in the presence of DPC, which probably relates to the charged head group of SDS. According to our data, other metals, such as sodium, magnesium, and calcium do not influence NRG1-III-Nct folding even in the presence of detergent (data not shown).

As secondary structure could be induced by a negatively charged detergent, we next tested the ability of lipid vesicles to induce NRG1-III-Nct folding. Partial folding into α helices occurred in the presence of a 1:1 lipid mixture of DMPC/DMPG together with 5 mM $ZnCl_2$ (Fig. 3d). Lipid vesicles, either DMPG/DMPG (Fig. 3d) or DOPC/DOPS (data not shown), alone were unable to induce conformational change. The interaction between the isolated NRG1-III-Nct and lipid membranes is likely to be relatively weak in the absence of the transmembrane domain, since

NRG1-III-Nct failed to co-sediment with lipid vesicles in ultracentrifugation (data not shown).

To rule out artefacts caused by the NRG1-III-Nct dimerization (see above), we also carried out SRCD with and without reducing agent. The result shows essentially identical conformational changes induced by SDS and Zn^{2+} (Fig. 3e), regardless of the presence of TCEP.

TFE is known to stabilize protein secondary structures, especially helices, and it is commonly used for protein folding and order–disorder studies (Buck 1998; Gast et al. 1999; Vassall et al. 2015). The folding state of NRG1-III-Nct was followed during a TFE titration. The protein showed helical conformation with increasing TFE concentration (Fig. 3f). This result is a sign of possible protein folding upon binding to an interaction partner, such as a membrane surface or metal ions. TFE lowers the solvent dielectric constant, thereby providing membrane-like conditions in solution.

NRG1-III-Nct binds to metal ions with micromolar affinity

To further investigate metal binding by NRG1-III-Nct, ITC experiments were performed. The binding assays (Fig. 4; Table 1) showed that the protein binds to Zn^{2+} as well as to Ni^{2+} with a dissociation constant K_d in the low micromolar range. No binding was observed with Mg^{2+} or Fe^{2+}. The results, together with SRCD data shown above, as well as the structural predictions, suggest a specific metal-binding site in the juxtamembrane segment of NRG1-III-Nct. The stoichiometries indicate 1:1 binding, and the binding event is strongly exothermic. The entropy contribution is very unfavourable, suggesting loss of structural flexibility upon binding. The ITC data indicate that NRG1-III-Nct interacts with certain metal ions also in the absence of a membrane-like environment, even though CD spectroscopy showed that this involves only minor, if any, changes in secondary structure.

Divalent metal ions are involved in myelination, and many myelin proteins also bind metals. Zinc binding myelin-specific proteins include for example MBP (Berlet et al. 1994) and the myelin-associated glycoprotein (MAG) (Kursula et al. 1999). The current view suggests that some metals, especially Zn^{2+}, may play a role in myelin protein binding to membrane surfaces (Wang et al. 2011). Such principles may also apply to other proteins peripherally attached to lipid membranes in other types of cellular environments.

The neuregulin cytoplasmic domain behaves like a random chain in solution

Synchrotron SAXS experiments were performed with the aim of getting more detailed 3D structural information

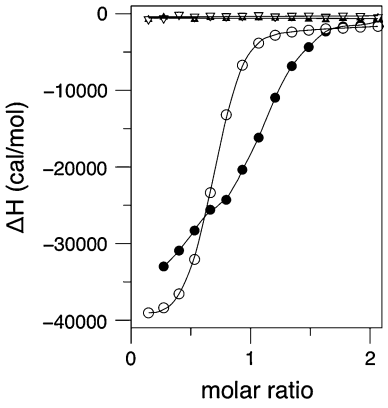

Fig. 4 Metal binding by NRG1-III-Nct ITC clearly indicates that NRG1-III-Nct binds Zn^{2+} (*solid circles*) and Ni^{2+} (*open circles*), but no signal is observed for Fe^{2+} or Mg^{2+} (*open* and *solid triangles,* respectively)

on NRG1-III-Nct (Figs. 5, 6; Table 2). SAXS is a method well suited for obtaining structural information on IDPs, including conformational changes and flexibility (Bernado and Svergun 2012). Two types of experiments were done: a highly concentrated batch of the protein was directly analysed (Fig. 5), and the protein was also subjected to an online SAXS experiment on a SEC column (Fig. 6). The latter was done to ensure separation of the monomeric and dimeric species.

The concentrated batch sample of NRG1-III-Nct provided good-quality SAXS data, which were used for structural analysis and modelling. During the analysis, it became evident that this sample behaved like a dimer, most likely linked by disulphide bridges. We decided, however, to build a dimeric model of the protein in the absence of high-concentration data from a monomeric sample. The featureless scattering curve (Fig. 5a) suggests a lack of globular folded domains, which is confirmed by the Kratky plot (Fig. 5b), clearly lacking any defined maximum characteristic for a folded protein.

For modelling NRG1-III-Nct, two approaches were used. The ensemble optimization method (EOM) was used to study conformational ensembles of NRG1-III-Nct (Fig. 5c, d). The fit to the raw data was better than with the single chain-like model, and the distributions of R_g and D_{max} closely resemble those for the entire pool of structures, built as disordered chains (Fig. 5c, d). Sometimes, IDPs present bimodal distributions of conformations (Ruskamo et al. 2012); the dimeric NGR1-III-Nct, however, is monomodal, and the SAXS data provide no evidence for a more compact molecular state. The most elongated conformations are in the range of $D_{max} = 150$ Å, which also fits the D_{max} estimation from the distance distribution function (Table 2).

Chain-like ab initio models were built using GASBOR (Fig. 5e, f); while we are aware that such flexible

Table 1 Metal ion-binding analysis by ITC

Ligand	Binding	Stoichiometry	K_d (μM)	ΔH (kcal/mol)	$-T\Delta S$ (kcal/mol)	ΔG (kcal/mol)
Zn^{2+}	Yes	1.04	1.9	−36.6	+28.8	−7.8
Ni^{2+}	Yes	0.65	0.5	−39.2	+30.7	−8.5
Fe^{2+}	No	–	–	–	–	–
Mg^{2+}	No	–	–	–	–	–

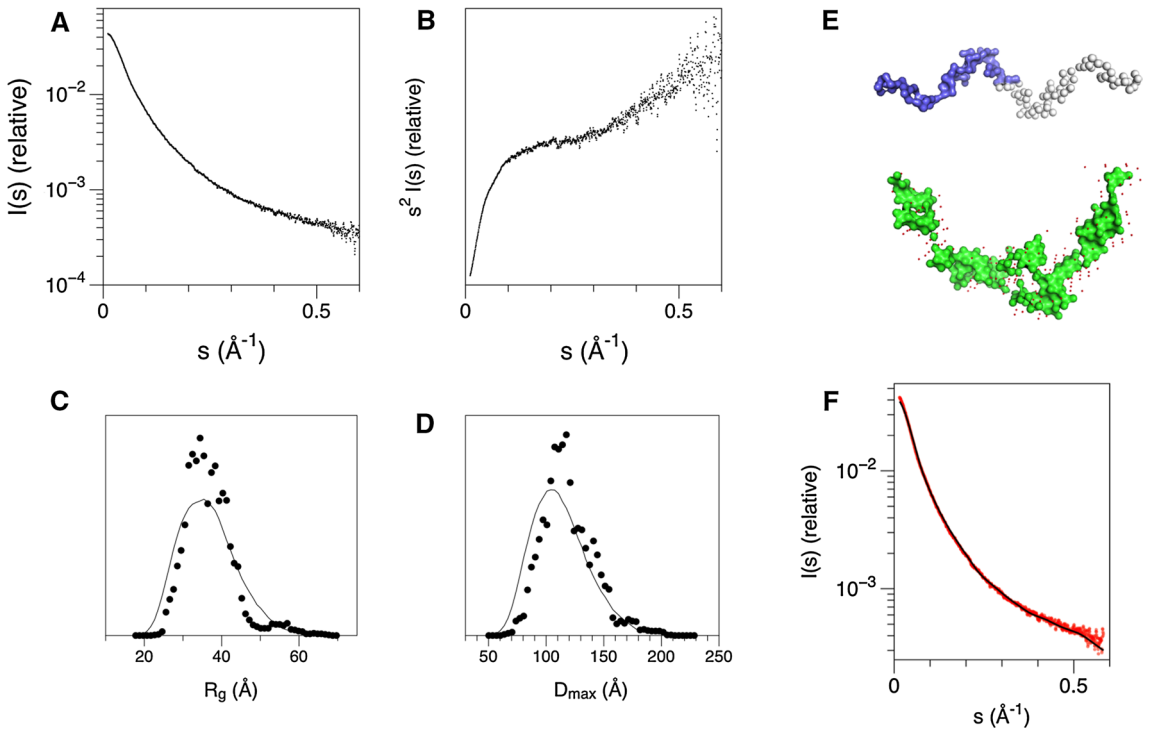

Fig. 5 SAXS analysis of NRG1-III-Nct in batch mode. **a** Raw scattering data collected in batch mode at high concentration. **b** Kratky plot. **c** R_g distribution of the EOM ensemble (*circles*) and the overall pool of disordered structures (*line*). **d** D_{max} distributions from EOM. **e** The ab initio GASBOR (*top*) and Denfert (*bottom*) models of NRG1-III-Nct. In the GASBOR model, the two chains, linked by a disulphide bridge near the C terminus, are shown as *blue surface* and *white spheres*. The maximum dimension of both models is approximately 100 Å, which locates them in the most populated region of the D_{max} distribution in panel D. **f** Fit (*black*) of the GASBOR model to the raw scattering data (*red*). For EOM and Denfert, the fits were even better (not shown; see χ^2 values in Table 2) (colour figure online)

IDPs cannot be reliably represented by a single model, we feel such a model gives a good view over the molecular dimensions. A single ab initio model can be taken as a data-compatible average molecular model. A dimeric model with P2 symmetry fit the data much better than a monomeric model. The best fit was obtained, when a mixture of monomer and dimer was modelled, although at the end, the fraction of monomer in the sample refined to only 2.5 %. Thus, the concentrated sample was mainly dimeric. The molecular weight estimated from the excluded volume of the ab initio model (19 kDa) also confirmed dimerization. Similar results and fits to raw data were also observed using the program Denfert (Fig. 5e). We conclude that in a concentrated sample exposed to X-rays, the reactivity of the free cysteine residues at the metal-binding site resulted in quantitative dimerization. However, this does not affect the reliability of the conclusion that the sample is an IDP.

In addition to the R_g values from Guinier plots, the Debye approximation was used, since it allows to use more data for the analysis in the case of an IDP (Table 2). For comparison, theoretical values of average R_g and D_{max} for a monomer and dimer random chain in the population were calculated based on polymer theory (Fitzkee and Rose 2004). For a monomeric random chain, expected values are $R_g = 26.8$ Å and $D_{max} = 79$ Å. For a dimer, these calculated values are $R_g = 40.8$ Å and $D_{max} = 112$ Å. Notably, the experimental (from EOM and GNOM) and theoretical values are highly similar, implying that NRG1-III-Nct behaves like a random polymer in solution.

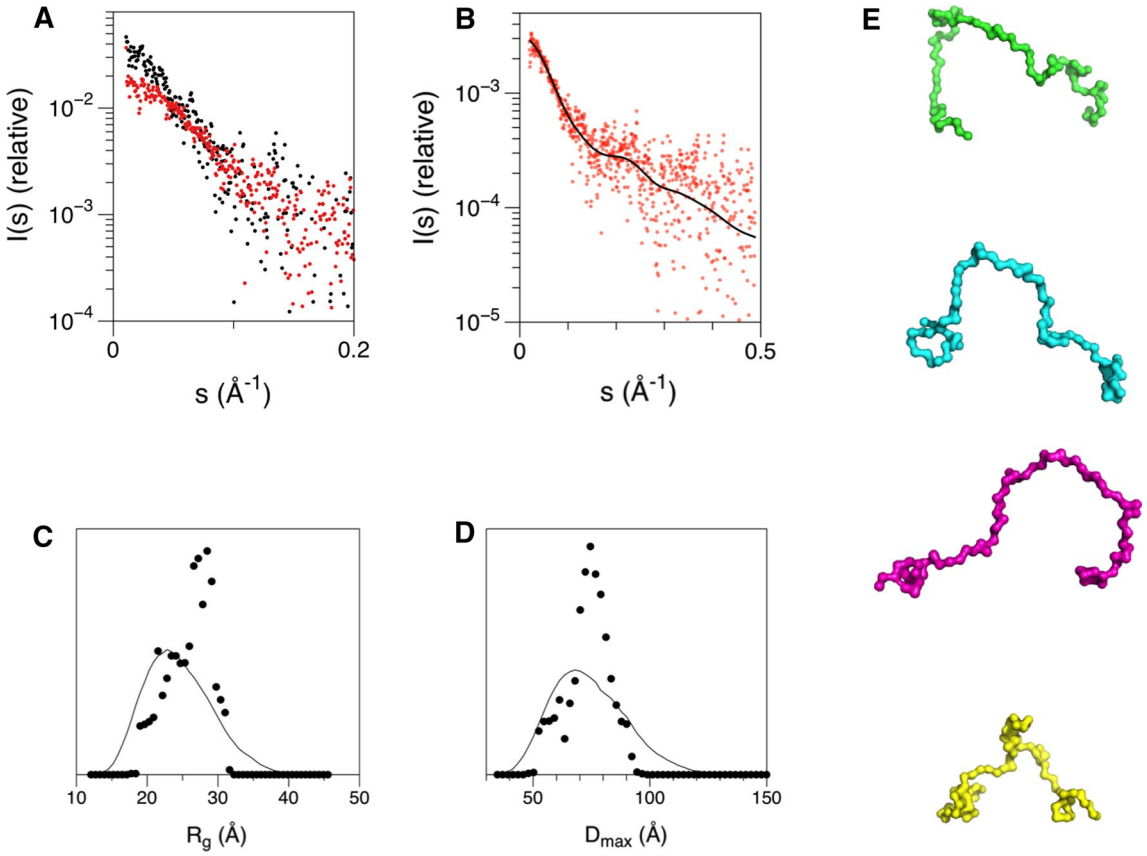

Fig. 6 Direct online SAXS analysis of the monomeric peak from gel filtration. **a** Scattering data from the monomer (*red*) and dimer (*black*) peaks in a SEC run. The difference in forward scattering intensity (I_0) clearly shows a twofold difference in molecular weight between the peaks. **b** Fit of the EOM structural ensemble (*black*) to the raw data (*red*) from the monomer peak. **c** R_g distribution of the EOM ensemble (*circles*) and the overall pool of disordered structures (*line*). **d** D_{max} distributions from EOM. **e** Four different conformations from the selected EOM ensemble, with R_g values between 20.8 and 30.0 Å and D_{max} between 59 and 87 Å (colour figure online)

Table 2 SAXS data analysis

Sample	R_g (Å) Guinier	R_g (Å) Debye	D_{max} (Å) GNOM	R_g (Å) EOM	D_{max} (Å) EOM	χ^2 GASBOR	χ^2 EOM	χ^2 Denfert
Batch	35.4	36.8	130	37.4	120	2.26	0.50	1.07
Monomer	26	27.1	–	26.2	74.6	–	2.42	–
Dimer	38	39.7	–	–	–	–	–	–

For obtaining information on the conformational behaviour of monomeric NRG1-III-Nct, we attempted to analyse the SAXS data from the monomer peak (Fig. 6). A twofold difference in molecular mass for the dimer and monomer peaks was observed via their respective I_0 values (Fig. 6a). Despite the relatively noisy data from this diluted small protein, we could obtain R_g values and run an ensemble optimization analysis (Fig. 6b–e). The EOM ensemble for the monomeric SEC peak presented R_g and D_{max} parameters highly similar to a monomeric random chain (Table 2). Hence, in addition to the high-concentration SAXS data from the dimer sample, the monomeric sample further proves the IDP properties of NRG1-III-Nct. Taken together, all structural data indicate that the N-terminal cytoplasmic domain of NRG1 type III behaves like a random polymer in solution. However, ligand binding may induce disorder-to-order transitions, as shown by the metal- and membrane-binding data.

Concluding remarks

We have carried out the first structural biology experiments for the NRG1 type III N-terminal cytoplasmic domain.

NRG1-III-Nct is intrinsically disordered and flexible in solution, and shows indications of interactions with metal ions and/or lipid membranes. In the future, finding interaction partners for this cytoplasmic domain will allow an insight into its physiological functions. While most attention on the biological function of NRG1 type III has focused on the extracellular domain and its effects on Schwann cells, the cytoplasmic tail could have functions related to interactions with neuronal cytosolic components, localization of the full-length protein, or signal transduction across the neuronal plasma membrane.

Acknowledgments Synchrotron beamtime and user support at SOLEIL and ANKA are gratefully acknowledged. We also acknowledge the Biocenter Oulu Proteomics Core Facility for providing the necessary mass spectrometric instrumentation. We wish to thank Saray Gonzalez for help with protein expression and purification. This study was financially supported by grants from Academy of Finland, the Sigrid Jusélius Foundation, and the Emil Aaltonen Foundation. The synchrotron data collection was supported by funding from the European Community 7th Framework Programme (FP7/2007–2013) under Biostruct-X (grant agreement 283570).

Conflict of interest The authors declare that they have no conflicts of interest.

References

Banci L, Bertini I, Ciofi-Baffoni S, Janicka A, Martinelli M, Kozlowski H, Palumaa P (2008) A structural–dynamical characterization of human Cox17. J Biol Chem 283:7912–7920

Bennett-Lovsey RM, Herbert AD, Sternberg MJ, Kelley LA (2008) Exploring the extremes of sequence/structure space with ensemble fold recognition in the program Phyre. Proteins 70:611–625

Berlet HH, Bischoff H, Weinhardt F (1994) Divalent metals of myelin and their differential binding by myelin basic protein of bovine central nervous system. Neurosci Lett 179:75–78

Bernado P, Svergun DI (2012) Structural analysis of intrinsically disordered proteins by small-angle X-ray scattering. Mol Bio Syst 8:151–167

Bernado P, Mylonas E, Petoukhov MV, Blackledge M, Svergun DI (2007) Structural characterization of flexible proteins using small-angle X-ray scattering. J Am Chem Soc 129:5656–5664

Buchan DW, Minneci F, Nugent TC, Bryson K, Jones DT (2013) Scalable web services for the PSIPRED Protein Analysis Workbench. Nucleic Acids Res 41:W349–W357

Buck M (1998) Trifluoroethanol and colleagues: cosolvents come of age. Recent studies with peptides and proteins. Q Rev Biophys 31:297–355

Calmettes P, Durand D, Desmadril M, Minard P, Receveur V, Smith JC (1994) How random is a highly denatured protein? Biophys Chem 53:105–113

David G, Pérez J (2009) Combined sampler robot and high-performance liquid chromatography: a fully automated system for biological small-angle X-ray scattering experiments at the Synchrotron SOLEIL SWING beamline. J Appl Crystallogr 42:892–900

Erickson SL, O'Shea KS, Ghaboosi N, Loverro L, Frantz G, Bauer M, Lu LH, Moore MW (1997) ErbB3 is required for normal cerebellar and cardiac development: a comparison with ErbB2-and heregulin-deficient mice. Development 124:4999–5011

Falls DL (2003a) Neuregulins and the neuromuscular system: 10 years of answers and questions. J Neurocytol 32:619–647

Falls DL (2003b) Neuregulins: functions, forms, and signaling strategies. Exp Cell Res 284:14–30

Fitzkee NC, Rose GD (2004) Reassessing random-coil statistics in unfolded proteins. Proc Natl Acad Sci USA 101:12497–12502

Fleck D, van Bebber F, Colombo A, Galante C, Schwenk BM, Rabe L, Hampel H, Novak B, Kremmer E, Tahirovic S, Edbauer D, Lichtenthaler SF, Schmid B, Willem M, Haass C (2013) Dual cleavage of neuregulin 1 type III by BACE1 and ADAM17 liberates its EGF-like domain and allows paracrine signaling. J Neurosci 33:7856–7869

Garratt AN, Britsch S, Birchmeier C (2000) Neuregulin, a factor with many functions in the life of a schwann cell. Bio Essays 22:987–996

Gast K, Zirwer D, Muller-Frohne M, Damaschun G (1999) Trifluoroethanol-induced conformational transitions of proteins: insights gained from the differences between alpha-lactalbumin and ribonuclease A. Protein Sci 8:625–634

Hammarström M, Woestenenk EA, Hellgren N, Hård T, Berglund H (2006) Effect of N-terminal solubility enhancing fusion proteins on yield of purified target protein. J Struct Funct Genomics 7:1–14

Heermann S, Schwab MH (2013) Molecular control of Schwann cell migration along peripheral axons: keep moving! Cell Adh Migr 7:18–22

Jones DT, Cozzetto D (2015) DISOPRED3: precise disordered region predictions with annotated protein-binding activity. Bioinformatics 31:857–863

Karl T (2013) Neuregulin 1: a prime candidate for research into gene-environment interactions in schizophrenia? Insights from genetic rodent models. Front Behav Neurosci 7:106

Koutsioubas A, Pérez J (2013) Incorporation of a hydration layer in the 'dummy atom' ab initio structural modelling of biological macromolecules. J Appl Crystallogr 46:1884–1888

Kursula P, Meriläinen G, Lehto VP, Heape AM (1999) The small myelin-associated glycoprotein is a zinc-binding protein. J Neurochem 73:2110–2118

Lazarova T, Brewin KA, Stoeber K, Robinson CR (2004) Characterization of peptides corresponding to the seven transmembrane domains of human adenosine A2a receptor. Biochemistry 43:12945–12954

Linding R, Russell RB, Neduva V, Gibson TJ (2003) GlobPlot: exploring protein sequences for globularity and disorder. Nucleic Acids Res 31:3701–3708

Liu X, Hwang H, Cao L, Buckland M, Cunningham A, Chen J, Chien KR, Graham RM, Zhou M (1998a) Domain-specific gene disruption reveals critical regulation of neuregulin signaling by its cytoplasmic tail. Proc Natl Acad Sci USA 95:13024–13029

Liu X, Hwang H, Cao L, Wen D, Liu N, Graham RM, Zhou M (1998b) Release of the neuregulin functional polypeptide requires its cytoplasmic tail. J Biol Chem 273:34335–34340

Mei L, Xiong WC (2008) Neuregulin 1 in neural development, synaptic plasticity and schizophrenia. Nat Rev Neurosci 9:437–452

Michailov GV, Sereda MW, Brinkmann BG, Fischer TM, Haug B, Birchmeier C, Role L, Lai C, Schwab MH, Nave KA (2004) Axonal neuregulin-1 regulates myelin sheath thickness. Science 304:700–703

Muruganandam G, Burck J, Ulrich AS, Kursula I, Kursula P (2013) Lipid membrane association of myelin proteins and peptide segments studied by oriented and synchrotron radiation circular dichroism spectroscopy. J Phys Chem B 117:14983–14993

Myllykoski M, Baumgartel P, Kursula P (2012) Conformations of peptides derived from myelin-specific proteins in membrane-mimetic conditions probed by synchrotron radiation CD spectroscopy. Amino Acids 42:1467–1474

Mylonas E, Svergun DI (2007) Accuracy of molecular mass determination of proteins in solution by small-angle X-ray scattering. J Appl Crystallogr 40:245–249

Nave KA, Salzer JL (2006) Axonal regulation of myelination by neuregulin 1. Curr Opin Neurobiol 16:492–500

Perlin JR, Lush ME, Stephens WZ, Piotrowski T, Talbot WS (2011) Neuronal Neuregulin 1 type III directs Schwann cell migration. Development 138:4639–4648

Petoukhov MV, Franke D, Shkumatov AV, Tria G, Kikhney AG, Gajda M, Gorba C, Mertens HDT, Konarev PV, Svergun DI (2012) New developments in the ATSAS program package for small-angle scattering data analysis. J Appl Cryst 45:342–350

Piirainen H, Hellman M, Tossavainen H, Permi P, Kursula P, Jaakola VP (2015) Human adenosine A2a receptor binds calmodulin with high affinity in a calcium-dependent manner. Biophys J 108:903–917

Popovic M, De Biasio A, Pintar A, Pongor S (2007) The intracellular region of the Notch ligand Jagged-1 gains partial structure upon binding to synthetic membranes. FEBS J 274:5325–5336

Refregiers M, Wien F, Ta HP, Premvardhan L, Bac S, Jamme F, Rouam V, Lagarde B, Polack F, Giorgetta JL, Ricaud JP, Bordessoule M, Giuliani A (2012) DISCO synchrotron-radiation circular-dichroism endstation at SOLEIL. J Synchrotron Radiat 19:831–835

Romero P, Obradovic Z, Dunker AK (2004) Natively disordered proteins: functions and predictions. Appl Bioinformatics 3:105–113

Ruskamo S, Chukhlieb M, Vahokoski J, Bhargav SP, Liang F, Kursula I, Kursula P (2012) Juxtanodin is an intrinsically disordered F-actin-binding protein. Sci Rep 2:899

Sigalov AB, Hendricks GM (2009) Membrane binding mode of intrinsically disordered cytoplasmic domains of T cell receptor signaling subunits depends on lipid composition. Biochem Biophys Res Commun 389:388–393

Svergun DI (1992) Determination of the regularization parameter in indirect-transform methods using perceptual criteria. J Appl Crystallogr 25:495–503

Svergun DI, Petoukhov MV, Koch MH (2001) Determination of domain structure of proteins from X-ray solution scattering. Biophys J 80:2946–2953

van den Berg S, Lofdahl PA, Hard T, Berglund H (2006) Improved solubility of TEV protease by directed evolution. J Biotechnol 121:291–298

Vassall KA, Jenkins AD, Bamm VV, Harauz G (2015) Thermodynamic analysis of the disorder-to-alpha-helical transition of 18.5-kDa myelin basic protein reveals an equilibrium intermediate representing the most compact conformation. J Mol Biol. (**in press**)

Vasudevan SV, Schulz J, Zhou C, Cocco MJ (2010) Protein folding at the membrane interface, the structure of Nogo-66 requires interactions with a phosphocholine surface. Proc Natl Acad Sci USA 107:6847–6851

Velanac V, Unterbarnscheidt T, Hinrichs W, Gummert MN, Fischer TM, Rossner MJ, Trimarco A, Brivio V, Taveggia C, Willem M, Haass C, Mobius W, Nave KA, Schwab MH (2012) Bace1 processing of NRG1 type III produces a myelin-inducing signal but is not essential for the stimulation of myelination. Glia 60:203–217

Wang JY, Frenzel KE, Wen D, Falls DL (1998) Transmembrane neuregulins interact with LIM kinase 1, a cytoplasmic protein kinase implicated in development of visuospatial cognition. J Biol Chem 273:20525–20534

Wang JY, Miller SJ, Falls DL (2001) The N-terminal region of neuregulin isoforms determines the accumulation of cell surface and released neuregulin ectodomain. J Biol Chem 276:2841–2851

Wang C, Neugebauer U, Burck J, Myllykoski M, Baumgartel P, Popp J, Kursula P (2011) Charge isomers of myelin basic protein: structure and interactions with membranes, nucleotide analogues, and calmodulin. PLoS One 6:e19915

Weickert CS, Tiwari Y, Schofield PR, Mowry BJ, Fullerton JM (2012) Schizophrenia-associated HapICE haplotype is associated with increased NRG1 type III expression and high nucleotide diversity. Transl Psychiatry 2:e104

Zhang Z, Prentiss L, Heitzman D, Stahl RC, DiPino FJ, Carey DJ (2006) Neuregulin isoforms in dorsal root ganglion neurons: effects of the cytoplasmic domain on localization and membrane shedding of Nrg-1 type I. J Neurosci Res 84:1–12